

> REPLACE THIS LINE WITH YOUR MANUSCRIPT ID NUMBER (DOUBLE-CLICK HERE TO EDIT) <

Research on High Frequency Vibration Reduction Using Carrier Phase Shifted PWM for 4-module 3-Phase Permanent Magnet Synchronous Motor

Zicheng Liu *Member, IEEE*, She Yan, Haiyang Fang *Member, IEEE*,
Dong Jiang *Senior Member, IEEE*, Ronghai Qu *Fellow, IEEE*

Abstract—This paper investigates the effect of a Carrier Phase Shifted Pulse Width Modulation (CPS-PWM) on the vibration reduction of inverter-fed multi-phase permanent magnet synchronous motors(PMSMs). This approach reduces vibration by changing the order of the carrier harmonic-induced electromagnetic force on the stator. Experiments prove that this method can effectively suppress vibration at a specific carrier frequency, but the vibration reduction effect depends on the carrier frequency, the mode frequency of the motor and the phase-shifted angles.

Index Terms—Multi-phase motor, permanent magnet synchronous motor, Carrier Phase Shifted Pulse Width Modulation, high-frequency electromagnetic vibration

I. INTRODUCTION

Multiphase PMSMs fed by converters are widely used in energy conversion areas requiring high reliability like electric propulsion applications, due to the excellent fault tolerance capability [1-4]. However, when the converter is working under PWM, high-frequency harmonic currents are introduced into the stator windings, resulting in high-frequency(HF) electromagnetic(EM) force, and HF vibration, which destroys the stealth performance of the propulsion system.

In order to reduce the high frequency EM vibration introduced by the converter, many scholars have carried out research work from the perspective of changing the carrier frequency. Literature [5] pointed out that by changing the carrier frequency to avoid the natural frequency of the motor, HF vibration can be avoided. But for different motors, it is very difficult to select an appropriate carrier frequency. Literature [6] proposed a variable carrier frequency PWM strategy based on the rotor position, which broadened the harmonic current spectrum by changing the carrier frequency to reduce the value of HF harmonic current, and suppress the HF vibration. However, because these methods generally lack accurate analysis of motor vibration response, the variable carrier frequency may sometimes worsen the HF vibration [7].

Some scholars have also explored how to reduce HF vibration at a fixed carrier frequency. In reference [8], for dual three-phase motors powered by parallel inverters, a PWM

method with a carrier phase shift of 90 degrees is proposed, which makes the phases of the harmonics at two times the carrier frequency in the two sets of three-phase windings opposite, effectively reducing HF vibration acceleration. Literature [9] sets a 180-degree phase shift on the carrier of the dual three-phase inverter, so that the harmonic phases at odd multiples of the carrier frequency in the two sets of three-phase windings are opposite, which reduces the HF vibration of the motor.

However, the above methods all rely on the cancellation of HF components in the magnetomotive force generated by the dual three-phase windings. This requires special designs such as common slots or interval slots for the dual three-phase windings of the motor, which severely limits the methods when extended to other types of motors.

In short, current researches usually focus on the frequency and magnitude of EM force, ignoring the influence of the spatial order of EM force on vibration. There lacks research on vibration reduction by adjusting the order of EM force.

This paper proposes a carrier phase shifted method for 4*3-phase PMSMs. The order of EM force is adjusted by carrier phase shift to suppress vibration. Firstly, the 4-module 3-phase PMSM and drive system were introduced, along with the analysis of the EM force. Then the vibration reduction mechanism of CPS-PWM was explained theoretically, considering the orders of HF EM forces. Finally, experimental results are agreed with the prediction of the theory and indicate that this approach can significantly reduce HF vibration under certain conditions.

II. THE MODEL OF 4-MODULE 3-PHASE PMSM

Fig. 1 shows the structure of the 4- module 3-phase PMSM. The motor has four sets of windings which occupy four sectors of the stator respectively. So the mutual inductance among different sets of windings is small. The electrical angles of different sets of windings differ by 0° .

This work was supported in part by the National Science and Foundation of China under Grant 52077088. (*Corresponding author: Haiyang Fang*)

> REPLACE THIS LINE WITH YOUR MANUSCRIPT ID NUMBER (DOUBLE-CLICK HERE TO EDIT) <

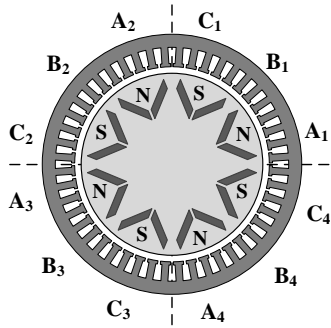


Fig. 1. Structure of the 4-module 3-phase PMSM

Fig. 2 shows the 4-module PMSM drive system. The system consists of four sets of three-phase voltage source inverters(VSIs) and a 4-module PMSM. Each set of windings of the motor is fed by a three-phase VSIs respectively. Therefore, each set of windings can be independently controlled.

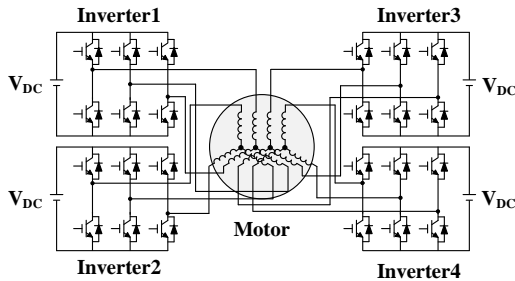


Fig.2. Schematic of 4-module PMSM drive system

III. ANALYSIS OF HIGH-FREQUENCY ELECTROMAGNETIC FORCE OF PMSM

The HF EM vibration of the motor is mainly generated by the HF EM force acting on the stator [10]. For PMSM, the HF EM force induced by PWM can be expressed as [11]:

$$f_{pwm}(\theta, t) = \sum_v \sum_\omega f_{v,\omega} \cos(v\theta - \omega t + \varphi) \quad (1)$$

$$v = 0, 2p \quad (2)$$

$$\omega = m\omega_c \pm n\omega_o (m \geq 1, n \geq 0) \quad (3)$$

$$\varphi = m\theta_c \pm n\theta_o \quad (4)$$

where v , ω and φ stand for the spatial order, angular frequency and phase of the EM force, respectively. p is the pole pairs number of the motor. ω_c and ω_o are the angular frequencies of the carrier and modulation wave, respectively. m , n are the index coefficient of the carrier and modulation wave. θ_c and θ_o are the phase of the carrier and modulation wave, respectively.

Formula (2) shows the spatial distribution of the EM force. It should be noted that: Formula (2) only applies to integer slot motors. For fractional slot motors, the spatial order of the HF EM force is very complex, which needs to be analyzed in combination with the specific motor structure.

Formula (3) shows the frequency characteristics of HF EM force under the Sinusoidal PWM(SPWM): concentrated on integral multiples of the carrier frequency. In Formula (3),when m is odd, n is 1,3,5,7,9.... When m is even, n is

0,2,4,6,8.... That can be expressed as:

$$\begin{cases} \omega = \omega_c \pm \omega_o, \omega_c \pm 3\omega_o, \dots \\ \omega = 2\omega_c, 2\omega_c \pm 2\omega_o, \dots \\ \dots \end{cases} \quad (5)$$

Formula (4) shows the phase characteristics of HF EM force. It can be seen from Formula (4) that the phase of the EM force can be changed by changing the phase of the carrier. The phase of the carrier changes X , the phase of EM force at m times the carrier frequency(mf_c) changes mX .

IV. THE MECHANISM OF VIBRATION GENERATION AND REDUCTION

A. Theoretical Analysis Vibration Generation:

Fig. 3 shows a typical mechanical transfer function curve of the motors. It can be obtained by modal experiment or finite element simulation. Decomposing the mechanical transfer function, the mechanical transfer function curve of each order mode can be obtained, as shown in Fig. 4.

The v -order transfer function in Fig. 4 can be expressed as:

$$H(v, \omega) = \frac{1}{\left[\left(\frac{\omega}{\omega_v} \right)^2 - 1 \right] + 2\zeta_v \frac{\omega}{\omega_v} i} = |H(v, \omega)| e^{j\theta_{v,w}} \quad (6)$$

$$|H(v, \omega)| = \sqrt{\left[\left(\frac{\omega}{\omega_v} \right)^2 - 1 \right]^2 + (2\zeta_v \frac{\omega}{\omega_v})^2} \quad (7)$$

where ω_v and ζ_v are the natural frequency and damping ratio of the v -order mode, respectively. Obviously the overall mechanical transfer function in Fig. 3 can be expressed as $\sum_v H(v, \omega)$.

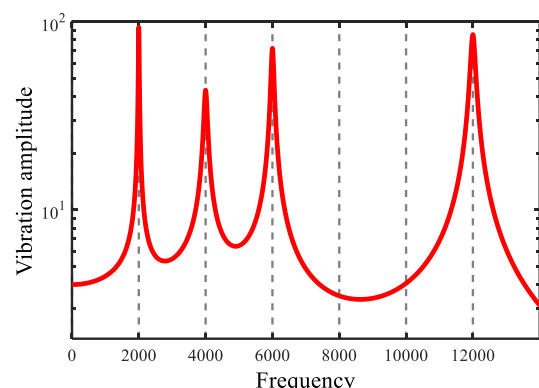
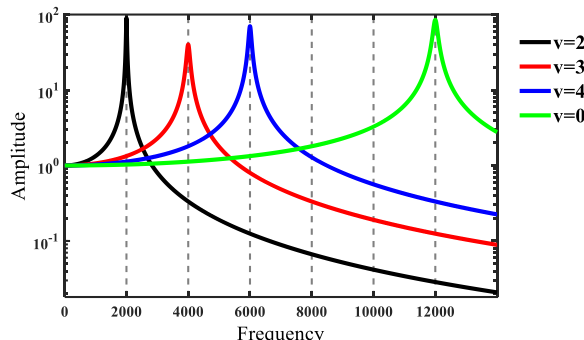
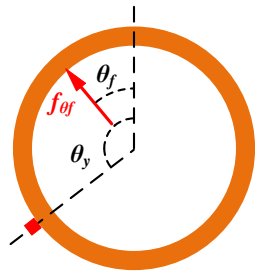


Fig. 3. Overall mechanical transfer function curve

> REPLACE THIS LINE WITH YOUR MANUSCRIPT ID NUMBER (DOUBLE-CLICK HERE TO EDIT) <

**Fig. 4.** Decomposed mechanical transfer function curve**Fig. 5.** Schematic diagram of the forces on the stator

In order to simplify the analysis, the motor stator is simplified as a ring, as shown in Fig. 5.

From Formula (1), it can be known that the μ -order HF EM force density can be expressed as:

$$f_\mu = f_{m\mu} \cos(\mu\theta - \omega t + \varphi_\mu) \quad (8)$$

As shown in Fig. 5, the EM force at point θ_f is expressed as:

$$f_{\theta_f} = f_{m\mu} \cos(\mu\theta_f - \omega t + \varphi_\mu) d\theta_f \quad (9)$$

The vibration response it produces at point θ_y is:

$$\begin{aligned} y &= f_{\theta_f} \times \sum_v H(v, \omega) \\ &= f_{m\mu} \cos(\mu\theta_f - \omega t + \varphi_\mu) d\theta_f \times \sum_v H(v, \omega) \\ &= \sum_v f_{m\mu} |H(v, \omega)| \cos[\mu\theta_f + v(\theta_y - \theta_f) - \omega t + \varphi_{u,v,\omega}] d\theta_f \end{aligned} \quad (10)$$

The vibration response produced by the total μ -order EM force at point θ_y is:

$$\begin{aligned} Y &= \int_0^{2\pi} f_{m\mu} |H(v, \omega)| \cos[\mu\theta_f + v(\theta_y - \theta_f) - \omega t + \varphi_{u,v,\omega}] d\theta_f \\ &= \sum_v f_{m\mu} |H(v, \omega)| \int_0^{2\pi} \cos[\mu\theta_f + v(\theta_y - \theta_f) - \omega t + \varphi_{u,v,\omega}] d\theta_f \end{aligned} \quad (11)$$

when $\mu \neq v$:

$$\begin{aligned} f_{m\mu} |H(v, \omega)| \int_0^{2\pi} \cos[\mu\theta_f + v(\theta_y - \theta_f) - \omega t + \varphi_{u,v,\omega}] d\theta_f \\ &= f_{m\mu} |H(v, \omega)| \int_0^{2\pi} \cos[(\mu - v)\theta_f + v\theta_y - \omega t + \varphi_{u,v,\omega}] d\theta_f \\ &= f_{m\mu} |H(v, \omega)| \times 0 \\ &= 0 \end{aligned} \quad (12)$$

That is, the v -order mode must be excited by the same order of EM force to generate vibration [12].

Therefore, Formula (11) can be simplified as:

$$\begin{aligned} Y &= f_{m\mu} |H(\mu, \omega)| \int_0^{2\pi} \cos[\mu\theta_f + \mu(\theta_y - \theta_f) - \omega t + \varphi_{\mu,v,\omega}] d\theta_f \\ &= 2\pi f_{m\mu} |H(\mu, \omega)| \cos(\mu\theta_y - \omega t + \varphi_{\mu,v,\omega}) \end{aligned} \quad (13)$$

The EM force with multiple spatial orders can be expressed as:

$$\begin{aligned} F &= \sum_\mu f_\mu \\ &= \sum_\mu f_{m\mu} \cos(\mu\theta - \omega t + \varphi_\mu) \end{aligned} \quad (14)$$

Combined with Formula (13), the vibration it generates at point θ_y can be expressed as:

$$\begin{aligned} Y &= \sum_\mu 2\pi f_{m\mu} |H(\mu, \omega)| \cos(\mu\theta_y - \omega t + \varphi_{\mu,v,\omega}) \\ &= \sum_\mu |Y_\mu| \cos(\mu\theta_y - \omega t + \varphi_{\mu,v,\omega}) \end{aligned} \quad (15)$$

$$|Y_\mu| = 2\pi f_{m\mu} |H(\mu, \omega)| \quad (16)$$

B. The Mechanism of Vibration Reduction:

For the HF EM force with frequency f_s , spatial order 0, and amplitude f_m , the vibration amplitude it produces is:

$$|Y_0| = 2\pi f_m |H(0, \omega_s)| \quad (17)$$

Change the order of the EM force, for example: change the order of the EM force to 2 without changing its amplitude and frequency, the vibration amplitude generated by it is:

$$|Y_2| = 2\pi f_m |H(2, \omega_s)| \quad (18)$$

When the EM force frequency f_s is close to the 0-order mode natural frequency f_{n0} , it can be seen from Fig. 4 that:

$$|H(0, \omega_s)| = |H(0, \omega_{n0})| \gg |H(2, \omega_{n0})| = |H(2, \omega_s)| \quad (19)$$

$$2\pi f_m |H(0, \omega_s)| \gg 2\pi f_m |H(2, \omega_s)| \quad (20)$$

$$|Y_0| \gg |Y_2| \quad (21)$$

That is, by changing the order of the EM force, the vibration generated by it would be greatly reduced.

V. CARRIER PHASE SHIFTED PWM AND VIBRATION REDUCTION

A. How Carrier Phase Shifted PWM Changes the Order of the Electromagnetic Force:

It can be seen from Chapter 1 that each module of the 4-module 3-phase motor is independent of each other, so the EM force generated by each module is also decoupled. Therefore, by changing the phase of the carrier of each module, the phase of the EM force generated by each module is changed.

As shown in Fig. 6, taking the carrier of the first module as a reference, set the carrier phases of the second to fourth module as θ_2 , θ_3 , θ_4 , and record this carrier phase combination(CPC) as $0 - \theta_2 - \theta_3 - \theta_4$.

It can be seen from Formula (4) that when the CPC is $0 - \frac{180}{m}$, the phase combination of EM force at around mf_c is $0 - \frac{180}{m}$, the phase combination of EM force at around mf_c is $0 - \frac{180}{m}$.

> REPLACE THIS LINE WITH YOUR MANUSCRIPT ID NUMBER (DOUBLE-CLICK HERE TO EDIT) <

180-0-180. At this time, the order of EM force at around mf_c changes from 0 to 2, as shown in Fig. 7.

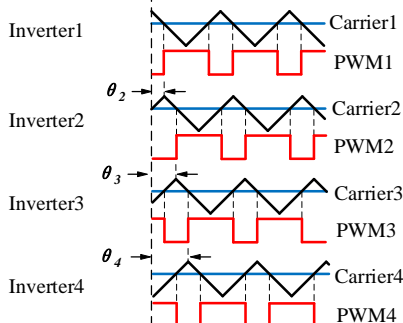


Fig. 6. Schematic diagram of CPS-PWM

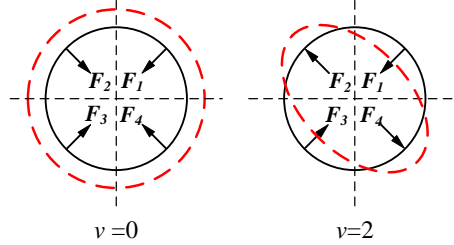


Fig. 7. Change of the order of the EM force

B. The Relationship between the Electromagnetic Force Order and the Carrier Phase Combination

It can be seen from Formula (2) that before the CPS-PWM is used, the main orders of the electromagnetic force are 0-order and $2p$ -order. The higher the order, the smaller the vibration generated by the EM force[13]. Therefore, the $2p$ -order electromagnetic force is ignored, and it is considered that the electromagnetic force is all 0-order before using the CPS-PWM. So the EM force can be expressed as:

$$\begin{aligned} f_{pwm} &= f_m \cos(v\theta - \omega t + \varphi) \\ &= f_m \cos(0\theta - \omega t + m\theta_c \pm n\theta_b + \theta_0) \quad (22) \\ &= f_m \cos(-\omega t + m\theta_c + \theta_{o,n,t}) \end{aligned}$$

Next, the order change of the electromagnetic force is mainly analyzed. In order to simplify the analysis, the time variable t is ignored. Take $t=t_0$ so that:

$$f_{pwm} = f_m \cos(-\omega t_0 + m\theta_c + \theta_{o,n,t}) = f_m \quad (23)$$

For the EM force with frequency $m\omega_c \pm n\omega_o$, when the CPC is 0-X-0-X, its expression at time t_0 is:

$$\begin{cases} f_{pwm} = f_m & \theta \in [0, 90^\circ] \\ f_{pwm} = f_m \cos(mX) & \theta \in [90, 180^\circ] \\ f_{pwm} = f_m & \theta \in [180, 270^\circ] \\ f_{pwm} = f_m \cos(mX) & \theta \in [270, 360^\circ] \end{cases} \quad (24)$$

The amplitude of each order EM force can be obtained by performing fast Fourier transform(FFT) on Formula (24). And Formula (24) can also be expressed as:

$$\begin{aligned} f_{pwm} &= f_{m0} + f_{m1} \cos(\theta) + f_{m2} \cos(2\theta) + \dots \\ &= \sum_{\mu} f_{m\mu} \cos(\mu\theta) \quad (25) \end{aligned}$$

Although there are many kinds of CPCs, after analysis, only two kinds of CPCs are helpful for vibration suppression: 0-X-0-X and 0-0-X-X.

Fig. 8 and Fig. 9 show that when CPC is 0-X-0-X and 0-0-X-X, the relative amplitude of each order EM force at around mf_c varies with the carrier phase angle(CPA) X.

As shown in Fig. 8, when the CPS is 0-X-0-X, the order of the EM force is expressed as: $\mu = 0, 2, 6, 10, \dots$. The relative amplitude of the 0-order EM force decreases sinusoidally with the CPA X, and the relative amplitudes of the other-order EM forces increase sinusoidally with the CPA X. When the CPA X is $\frac{180^\circ}{m}$, the amplitude of the 0-order EM force is 0 and the 2-order EM force is dominant.

As shown in Fig. 9, when the CPS is 0-0-X-X, the order of the EM force is expressed as: $\mu = 0, 1, 3, 5, \dots$. In general, there is no 1-order mode of the motor[14], so the vibration generated by the 1-order EM force can be ignored. Therefore, ignoring the 1-order EM force, it is considered that when the CPA is $\frac{180^\circ}{m}$, the 3-order EM force is dominant.

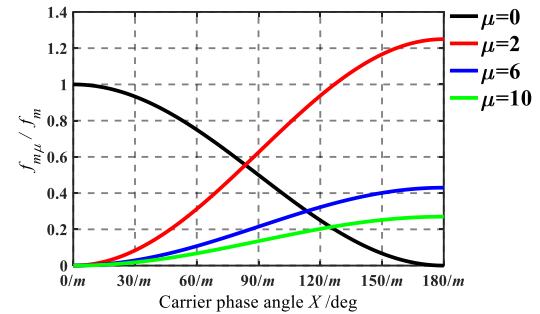


Fig. 8. Change of orders under CPC 0-X-0-X

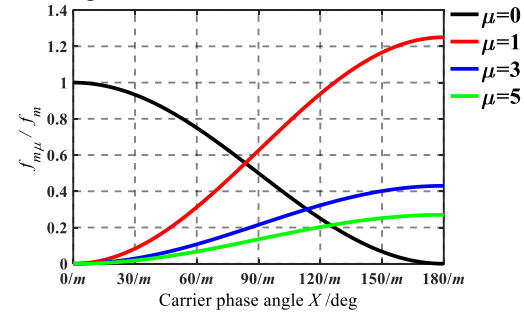


Fig. 9. Change of orders under CPC 0-0-X-X

VI. EXPERIMENTAL VALIDATION

To verify the above analysis, experiments are conducted on three different PMSMs, which are a 4-module PMSM(motor 1) with 48 slots and 8 poles, a 2-module PMSM(motor 2) with 12 slots and 8 poles, and a 4-module PMSM(motor 3) with 12 slots and 16 poles. The following three groups of experiments are described in details:

A. Introduction to the experimental platform:

The structures of the three motors are shown in Fig. 10, Fig. 11 and Fig. 12. The basic parameters are shown in Table I, Table II and Table III.

> REPLACE THIS LINE WITH YOUR MANUSCRIPT ID NUMBER (DOUBLE-CLICK HERE TO EDIT) <

The experimental platform are shown in Fig. 13. Accelerometers are evenly arranged on the stator surface. Control the motor to run at a constant speed, measure the vibration acceleration, and obtain the vibration spectrums after analysis. Take the average of the vibration amplitudes measured by all sensors as the vibration result. Change the carrier frequency and CPCs, repeat the above steps, then compare the vibration results under different conditions.

The harmonic current at around $2f_c$ generated by the VSIs is the largest[15], so the vibration at around $2f_c$ is generally the largest. Therefore, focus on the change of the vibration at around $2f_c$.

Set the CPA X to $0^\circ, 10^\circ, 10^\circ, \dots, 90^\circ$, so that the phase of the EM force at around $2f_c$ changes from 0° to 180° .

The carrier frequency is taken as half of the natural frequency of the 0-order mode and the 3-order mode, which makes the vibration change obvious.

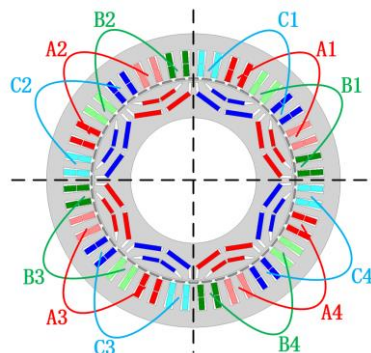


Fig. 10. Structure diagram of motor 1

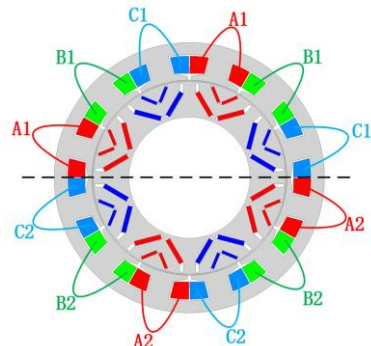


Fig. 11. Structure diagram of motor 2

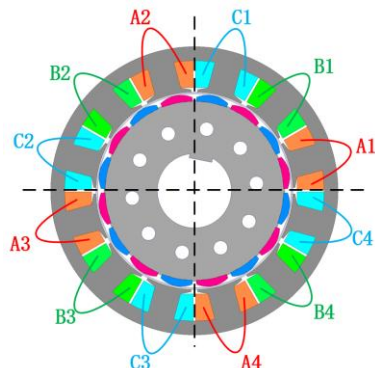


Fig. 12. Structure diagram of motor 3

TABLE I

PARAMETERS OF MOTORS			
Parameter	Motor1	Motor2	Motor3
Slot number	48	12	12
Pole number	8	8	16
Stator OD(mm)	180	180	124
Stator ID(mm)	124	130	85
Air gap(mm)	0.8	0.8	1.4
Rated power(kW)	15.67	15.77	3
Rated speed(rpm)	3000	3000	1000

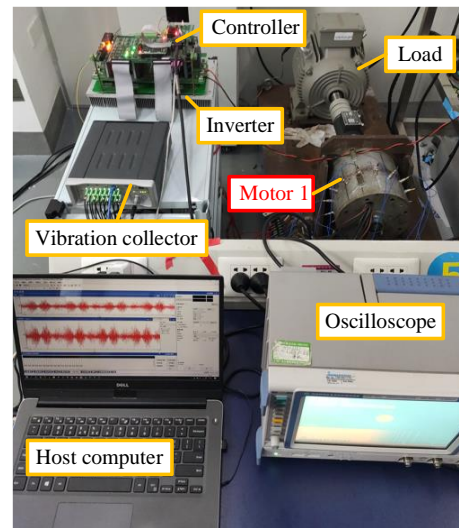


Fig. 13. Experimental platform for motors

B. Experimental results of motor 1:

The modal experiment is carried out on the motor, and the natural frequencies of the motor are shown in Table II.

TABLE II

NATURAL FREQUENCY OF MOTOR 1

Order	Natural Frequency/Hz
2	1990
3	3042
4	4577
0	20127

Fig. 14 shows the vibration spectrums under CPC 0-0-0-0 and CPC 0-90-0-90 when the carrier frequency is 10kHz. It can be seen from the spectrums that the vibration amplitude at around $2f_c$ is the largest. Comparing the two spectrums, we can see that in the case of 0-90-0-90, the vibration amplitude at around $2f_c$ is reduced by about 50%.

When $f_c = 10\text{kHz}$, there exists $2f_c \approx f_{n0}$, where f_{n0} is the 0-order mode natural frequency.

$$\text{Therefore: } |H(0, 2\omega_c)| \gg |H(3, 2\omega_c)| > |H(2, 2\omega_c)|.$$

When CPC is 0-0-0-0, the theoretical vibration amplitude around $2f_c$ is $|Y_{0-0-0-0}| = f_{m0} |H(0, 2\omega_c)| = f_m |H(0, 2\omega_c)|$.

When CPC is 0-90-0-90, the theoretical vibration amplitude around $2f_c$ is

> REPLACE THIS LINE WITH YOUR MANUSCRIPT ID NUMBER (DOUBLE-CLICK HERE TO EDIT) <

$$\begin{aligned} |Y_{0-90-0-90}| &= |f_{m2}H(2, 2\omega_c)| + |f_{m6}H(6, 2\omega_c)| + |f_{m10}H(10, 2\omega_c)| + \dots \\ &\approx f_{m2}|H(2, 2\omega_c)| \\ &= 1.25f_m|H(2, 2\omega_c)| \end{aligned}$$

Since $|H(0, 2\omega_c)| \gg |H(2, 2\omega_c)|$, so $|Y_{0-0-0-0}| \gg |Y_{0-90-0-90}|$.

Therefore, the vibration amplitude at around $2f_c$ is reduced in the case of 0-90-0-90.

It can be seen from Fig. 14 that the vibration is reduced by about 50%, and the vibration reduction effect is not as good as the theoretical analysis. This is mainly because: In the theoretical analysis, the motor stator is regarded as an ring without thickness. But the actual motor has a casing, coils, and it is a slotted design, which make the motor stator unable to be regarded as an ideal ring and affect the vibration reduction effect.

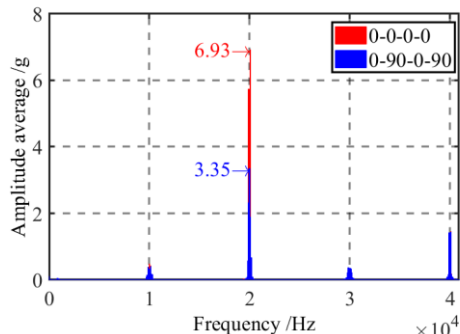


Fig. 14. Vibration spectrum when $f_c = 10\text{kHz} \approx f_{n0}/2$

Fig. 15 shows the vibration amplitudes at around $2f_c$ under different CPCs when the carrier frequency is 10kHz. As can be seen from the figure, as the CPA X increases, the vibration amplitude gradually decreases. In the case of the same CPA X, the vibration amplitude under 0-X-0-X is smaller than that under 0-0-X-X.

The vibration at around $2f_c$ can be expressed as:

$$\begin{aligned} |Y_{0-X-0-X}| &= f_{m0}|H(0, 2\omega_c)| + f_{m2}|H(2, 2\omega_c)| + f_{m6}|H(6, 2\omega_c)| \dots \\ &\approx f_{m0}|H(0, 2\omega_c)| + f_{m2}|H(2, 2\omega_c)| \end{aligned} \quad (26)$$

$$\begin{aligned} |Y_{0-0-X-X}| &= f_{m0}|H(0, 2\omega_c)| + f_{m1}|H(1, 2\omega_c)| + f_{m3}|H(3, 2\omega_c)| \dots \\ &\approx f_{m0}|H(0, 2\omega_c)| + f_{m3}|H(3, 2\omega_c)| \end{aligned} \quad (27)$$

As shown in Fig. 8 and Fig. 9, as the CPA X increases, the magnitude of the 0-order EM force f_{m0} gradually decreases, so the first term in Formula (26),(27) gradually decreases. Therefore, the vibration at $2f_c$ also decreases gradually.

Since $|H(2, 2\omega_c)| < |H(3, 2\omega_c)|$, the second term in Formula (26) is less than that in Formula (27), so the vibration amplitude under 0-X-0-X is smaller than that under 0-0-X-X.

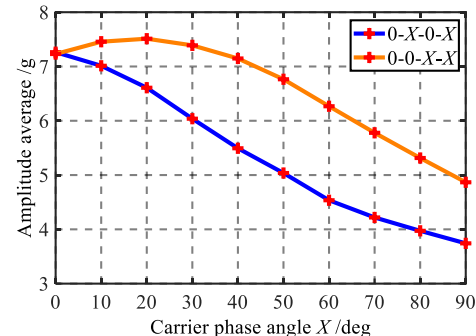


Fig. 15. Vibration Amplitude at around $2f_c$ versus CPA when $f_c = 10\text{kHz} \approx f_{n0}/2$

Fig. 16 shows the vibration spectrums under CPC 0-0-0-0 and CPC 0-0-90-90 when the carrier frequency is 1500Hz. We can see that in the case of 0-0-90-90, the vibration amplitude at around $2f_c$ increased by 30 times.

When $f_c = 1500\text{Hz}$, there are: $2f_c \approx f_{n3}$, where f_{n0} is the 0-order mode natural frequency.

$$\text{Therefore: } |H(3, 2\omega_c)| \gg |H(2, 2\omega_c)| \gg |H(0, 2\omega_c)|.$$

When CPC is 0-0-0-0, the theoretical vibration amplitude at around $2f_c$ is $|Y_{0-0-0-0}| = f_{m0}|H(0, 2\omega_c)| = f_m|H(0, 2\omega_c)|$.

When CPC is 0-0-90-90, the theoretical vibration amplitude at around $2f_c$ is

$$\begin{aligned} |Y_{0-0-90-90}| &= |f_{m1}H(1, 2\omega_c)| + |f_{m3}H(3, 2\omega_c)| + |f_{m5}H(5, 2\omega_c)| + \dots \\ &\approx f_{m3}|H(3, 2\omega_c)| \\ &= 0.43f_m|H(3, 2\omega_c)| \end{aligned}$$

Since $|H(3, 2\omega_c)| \gg |H(0, 2\omega_c)|$, so $|Y_{0-0-90-90}| \gg |Y_{0-0-0-0}|$.

Therefore, the vibration amplitude at around $2f_c$ is greatly increased in the case of 0-0-90-90.

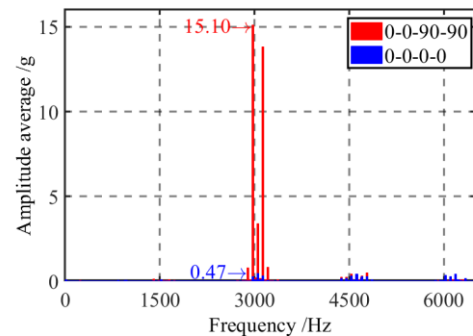


Fig. 16. Vibration spectrum when $f_c = 1500\text{Hz} \approx f_{n3}/2$

Fig. 17 shows the vibration amplitudes at around $2f_c$ under different CPCs when the carrier frequency is 1500Hz. As can be seen from the figure, as the CPA X increases, the vibration amplitude gradually increases. In the case of the same CPA X, the vibration amplitude under 0-X-0-X is smaller than that under 0-0-X-X.

Since $|H(3, 2\omega_c)| \gg |H(2, 2\omega_c)| \gg |H(0, 2\omega_c)|$, the vibration at around $2f_c$ can be expressed as:

> REPLACE THIS LINE WITH YOUR MANUSCRIPT ID NUMBER (DOUBLE-CLICK HERE TO EDIT) <

$$|Y_{0-X-0-X}| = f_{m0} |H(0, 2\omega_c)| + f_{m2} |H(2, 2\omega_c)| + f_{m6} |H(6, 2\omega_c)| \dots \quad (28)$$

$$\approx f_{m2} |H(2, 2\omega_c)|$$

$$|Y_{0-0-X-X}| = f_{m0} |H(0, 2\omega_c)| + f_{m1} |H(1, 2\omega_c)| + f_{m3} |H(3, 2\omega_c)| \dots \quad (29)$$

$$\approx f_{m3} |H(3, 2\omega_c)|$$

As shown in Fig. 8 and Fig. 9, as the CPA X increases, f_{m2} and f_{m3} gradually increase. Therefore, the vibration at $2f_c$ also decreases gradually.

Since $|H(2, 2\omega_c)| < |H(3, 2\omega_c)|$, so the vibration amplitude under 0-X-0-X is smaller than that under 0-0-X-X.

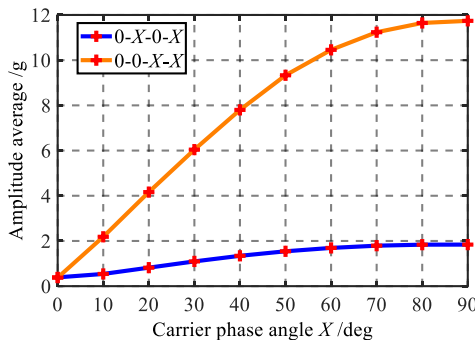


Fig. 17. Vibration Amplitude at around $2f_c$ versus CPA when $f_c = 1500\text{Hz} \approx f_{n3} / 2$

C. Experimental results of 12-slot 8-pole motor:

The modal experiment is carried out on the motor, and the natural frequencies of the motor are shown in Table III.

TABLE III

NATURAL FREQUENCY OF MOTOR 2

Order	Natural Frequency/Hz
2	2394
3	3434
4	5428
0	25207

The motor is a 2-module motor, so there is only one type of CPC, namely 0-X. It can be seen from the motor structure in Fig. 11 that 0-X in the two-module motor can be equivalent to 0-0-X-X in the four-module motor.

Experiments were carried out when the carrier frequency was 1700 Hz and 12500 Hz. The experimental results are shown in Fig. 18, Fig. 19 and are very similar to the experimental results of motor A.

The motor used is a fractional slot concentrated winding motor, and the spatial order of the EM force is relatively complex, not only containing 0-order. However, it can be seen from Fig. 18 that the vibration can still be reduced by using CPS-PWM, although the vibration suppression effect is not as good as that of integer slot motors.

Similarly, when the carrier frequency of 2 times is close to the natural frequency of the 3-order mode, using the CPS-PWM, the HF vibration is greatly increased.

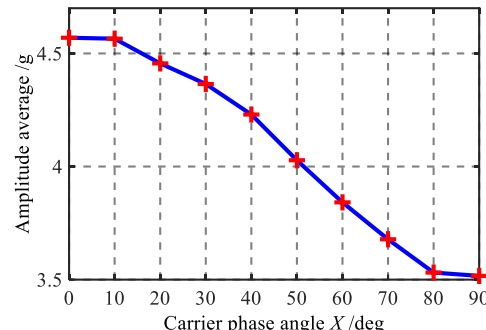


Fig. 18. Vibration Amplitude at around $2f_c$ versus CPA when $f_c = 12.5\text{kHz} \approx f_{n0} / 2$

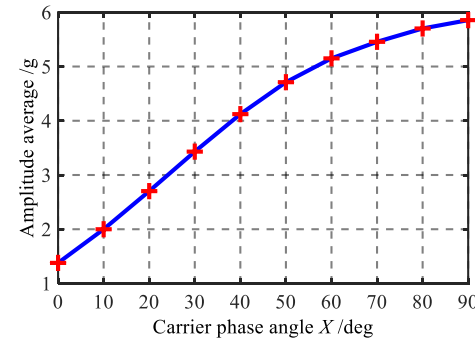


Fig. 19. Vibration Amplitude at around $2f_c$ versus CPA when $f_c = 1700\text{Hz} \approx f_{n3} / 2$

D. Experimental results of 12-slot 16-pole motor:

The modal experiment is carried out on the motor, and the natural frequencies of the motor are shown in Table IV.

TABLE IV

NATURAL FREQUENCY OF MOTOR 3

Order	Natural Frequency/Hz
2	2312
3	3263
4	4940
0	18137

Experiments were carried out when the carrier frequency was 1600 Hz and 9000 Hz. The experimental results are shown in Fig. 20, Fig. 21 and are very similar to the experimental results of motor 1.

The motor used is a fractional slot concentrated winding motor, and each module contains two pairs of magnetic poles. However, it can be seen from Fig. 20 that the vibration can still be reduced by using CPS-PWM.

Through the above three sets of motor experiments, it can be seen that the structure of the PMSM does not affect the vibration suppression effect of CPS-PWM. As long as the motor is a multi-module PMSM, the HF EM vibration can be suppressed by the using the proper CPS-PWM.

> REPLACE THIS LINE WITH YOUR MANUSCRIPT ID NUMBER (DOUBLE-CLICK HERE TO EDIT) <

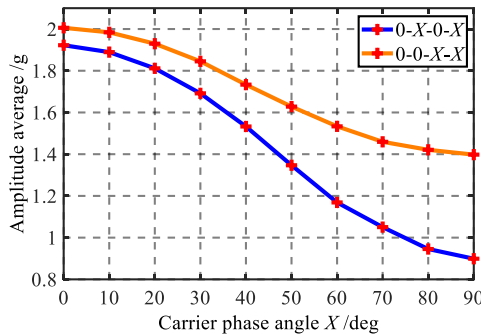


Fig. 20. Vibration Amplitude at around $2f_c$ versus CPA when $f_c = 9000\text{Hz} \approx f_{n0} / 2$

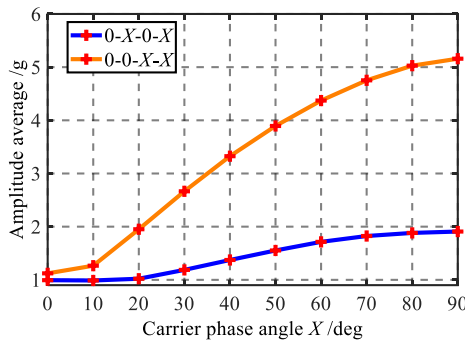


Fig. 21. Vibration Amplitude at around $2f_c$ versus CPA when $f_c = 1600\text{Hz} \approx f_{n3} / 2$

VII. CONCLUSION

This paper provides a new HF PWM EM vibration suppression method, which can suppress vibration by changing the order of the EM force. In this paper, the principle of vibration suppression is theoretically analyzed, and the effectiveness of the method is verified by experiments. The following conclusions can be drawn.

- 1) At a specific carrier frequency, that is, when the carrier frequency multiplier is close to the 0-order mode natural frequency, the HF vibration of the multi-module motor can be effectively reduced by using proper CPS-PWM. However, when the carrier frequency multiplier is close to the natural frequency of the 2-order or 3-order mode, the HF vibration may increase under CPS-PWM.
- 2) The 0-order EM force can be transformed to the 2-order or 3-order force by the CPS-PWM of 0-X-0-X or 0-0-X-X. The order of the main EM force under 0-X-0-X is lower, so 0-X-0-X is better at HF vibration reduction.
- 3) This vibration suppression method is suitable for multi-module PMSMs and is not affected by the structure of the stator or rotor. But the EM force order distribution of integer slot motor is relatively simple, and therefore the vibration suppression effect of integer slot motor is better.

ACKNOWLEDGMENT

This work is supported by the National Natural Science Foundation of China under Project 52077088.

REFERENCES

- [1] S. Yan, Q. Wang, Y. Xu, Z. Liu, H. Fang and D. Jiang, "Research on High Frequency Vibration Reduction Using Carrier Phase Shifted PWM for 4 3-Phase Windings Permanent Magnet Synchronous Motor," 2021 IEEE Energy Conversion Congress and Exposition (ECCE), Vancouver, BC, Canada, 2021, pp. 4468-4472.
- [2] A. Mohammadpour and L. Parsa, "Global Fault-Tolerant Control Technique for Multiphase Permanent-Magnet Machines," in IEEE Transactions on Industry Applications, vol. 51, no. 1, pp. 178-186, Jan.-Feb. 2015.
- [3] Z. Liu, L. Fang, D. Jiang and R. Qu, "A Machine-learning Based Fault Diagnosis Method with Adaptive Secondary Sampling for Multiphase Drive Systems," in IEEE Transactions on Power Electronics, vol. 36, no. 1, pp. 111172, Sep. 2021.
- [4] X. Peng, Z. Liu, and D. Jiang, "A review of multiphase energy conversion in wind power generation," Renewable and Sustainable Energy Reviews, vol. 147, p. 111172, Sep. 2021.
- [5] E. Zeze, and K. Akatsu, "Research on vibration analysis and noise-reduction technique of PM motor," in 2012 XXth International Conference on Electrical Machines, Marseille, 2012, pp. 458-463.
- [6] Zhi Yang, S. Yaman and M. Krishnamurthy, "Mitigation of EM vibration in PMSM: A rotor position related variable carrier frequency technique," in 2017 IEEE Transportation Electrification Conference and Expo (ITEC), Chicago, IL, 2017, pp.448-452.
- [7] I. P. Tsoumas, and H. Tischmacher, "Influence of the inverter's modulation technique on the audible noise of electric motors," in 2012XXth International Conference on Electrical Machines, Marseille, 2012, pp. 2981-2987.
- [8] F. Yuan, S. Huang, and Q. Hao, "Research on High Frequency Vibration Suppression of Permanent Magnet Motor Using Carrier Phase Shift Technology," in Electric Machines and Control, 2014, (7):12-17.
- [9] W. Zhang, Y. Xu, H. Huang and J. Zou, "Vibration Reduction for Dual-Branch Three-Phase Permanent Magnet Synchronous Motor With Carrier Phase-Shift Technique," in IEEE Transactions on Power Electronics, vol. 35, no. 1, pp. 607-618, Jan. 2020.
- [10]X. Li, C. Liu, and B. Mei, "Analysis of Vibration and Noise Source of Electric Vehicle IPMSM Wide Range Speed Regulation," in Electric Machines and Control, 2018, 38(17):5219-5227+5319.
- [11]C. Liao, W. Jiang and Z. Zhang, "Analysis of EMVibration Characteristics of An Interior Permanent Magnet Synchronous Motor," in 2019 22nd International Conference on Electrical Machines and Systems (ICEMS), Harbin, China, 2019, pp.1-5.
- [12]S. Wang, J. Hong, Y. Sun and H. Cao, "Analysis of Zeroth-Mode Slot Frequency Vibration of Integer Slot Permanent-Magnet Synchronous Motors," in IEEE Transactions on Industrial Electronics, vol. 67, no. 4, pp. 2954-2964, April 2020.
- [13]Y. -S. Lai, W. -T. Lee, Y. -K. Lin and J. -F. Tsai, "Integrated Inverter/Converter Circuit and Control Technique of Motor Drives With Dual-Mode Control for EV/HEV Applications," in IEEE Transactions on Power Electronics, vol. 29, no. 3, pp. 1358-1365, March 2014.
- [14]G. Vidmar and D. Miljavec, "A Universal High-Frequency Three-Phase Electric-Motor Model Suitable for the Delta- and Star-Winding Connections," in IEEE Transactions on Power Electronics, vol. 30, no. 8, pp. 4365-4376, Aug. 2015.
- [15] Pulse Width Modulation for Power Converters Principles and Practice[M]. John Wiley & Sons Inc, 2003.



Zicheng Liu (M'18) was born in Shandong, China, in 1989. He received the B.S. degree in Hydropower Engineering from Huazhong University of Science and Technology (HUST), Wuhan, China, in 2011, and the Ph.D. degree in Electrical Engineering from Tsinghua University, Beijing, China, in 2016. During Oct. 2014 to Mar. 2015, he was a Visiting Student at Purdue University, West Lafayette, IN, USA. During Jun. 2016 to Sep. 2018, he was a postdoc researcher at Beijing Jiaotong University, Beijing, China. He is currently an associate professor at HUST. His research interests include multiphase motor control systems and transportation electrification.

> REPLACE THIS LINE WITH YOUR MANUSCRIPT ID NUMBER (DOUBLE-CLICK HERE TO EDIT) <



She Yan was born in Jiangxi, China, in 1999. He received the B.S. degree in Electrical Engineering from the Huazhong University of Science and Technology, Wuhan, China, in 2021, where he is currently working toward the M.S. degree in Electrical Engineering with the School of Electronic and Electrical Engineering. His main research interests are motor control and motor vibration.



Haiyang Fang (Member, IEEE) was born in Hubei, China. He received the B.M.E. degree in mechanical engineering and the Ph.D. degree in electrical engineering from the Huazhong University of Science and Technology, Wuhan, China, in 2013 and 2018, respectively. His research interests include mechanical design and vibro-acoustic analysis of electrical machines.



Dong Jiang (S05'-M12'-SM16') received B.S and M.S degrees in electrical engineering from Tsinghua University, Beijing, China, in 2005 and 2007 respectively. He began his Ph.D. study in Center for Power Electronics Systems (CPES) in Virginia Tech in 2007 and was transferred to University of Tennessee with his advisor in 2010. He received his Ph.D. degree in power electronics and motor drives from University of Tennessee in Dec. 2011. He was with United Technologies Research Center (UTRC) in Connecticut as a Senior Research Scientist/Engineer from Jan 2012

to July 2015. He has been with Huazhong University of Science &Technology (HUST) in China as a professor since July 2015. Dong Jiang's major research area is power electronics and motor drives, with more than 40 published IEEE journal and conference papers in this area. He has two best paper awards in IEEE conferences. He is an associate editor of IEEE Transactions on Industry Applications.



Ronghai Qu (Fellow, IEEE) was born in China. He received the B.E.E. and M.S.E.E. degrees in electrical engineering from Tsinghua University, Beijing, China, in 1993 and 1996, respectively, and the Ph.D. degree in electrical engineering from the University of Wisconsin-Madison, Madison, WI, USA, in 2002. In 1998, he joined the Wisconsin Electric Machines and Power Electronics Consortiums as Research Assistant. He became a Senior Electrical Engineer with Northland, a Scott Fetzer Company in 2002. Since 2003, he had been with the General Electric (GE) Global Research Center, Niskayuna, NY, USA, as a Senior Electrical Engineer with the Electrical Machines and Drives Laboratory. He has authored more than 120 published technical papers and is the holder of more than 50 patents/patent applications. From 2010, he has been a Professor with the Huazhong University of Science &Technology, Wuhan, China. Prof. Qu is a full member of Sigma Xi. He has been the recipient of several awards from GE Global Research Center since 2003, including the Technical Achievement and Management Awards. He is also the recipient of the 2003 and 2005 Best Paper Awards, and third prize from the Electric Machines Committee of the IEEE Industry Applications Society at the 2002 and 2004 IAS Annual Meeting.

Research on High Frequency Vibration Reduction Using Carrier Phase Shifted PWM for 4-module 3-Phase Permanent Magnet Synchronous Motor

by SheYan

Submission date: 04-Apr-2022 08:31PM (UTC+0800)

Submission ID: 1801332949

File name: rBBVJ2JK5JmAE2cDADq-STUBcNM86.docx (3.67M)

Word count: 4401

Character count: 22474

5
> REPLACE THIS LINE WITH YOUR MANUSCRIPT ID NUMBER (DOUBLE-CLICK HERE TO EDIT) <

1

18

Research on High Frequency Vibration Reduction Using Carrier Phase Shifted PWM for 4-module 3-Phase Permanent Magnet Synchronous Motor

22

Zicheng Liu *Member, IEEE*, She Yan, Haiyang Fang *Member, IEEE*,

Dong Jiang *Senior Member, IEEE*, Ronghai Qu *Fellow, IEEE*

1

Abstract—This paper investigates the effect of a Carrier Phase Shifted Pulse Width Modulation (CPS-PWM) on the vibration reduction of inverter-fed multi-phase permanent magnet synchronous motors(PMSMs). This approach reduces vibration by changing the order of the carrier harmonic-induced electromagnetic force on the stator. Experiments prove that this method can effectively suppress vibration at a specific carrier frequency, but the vibration reduction effect depends on the carrier frequency, the mode frequency of the motor and the phase-shifted angles.

Index Terms—Multi-phase motor, permanent magnet synchronous motor, Carrier Phase Shifted Pulse Width Modulation, high-frequency electromagnetic vibration

1

three-phase motors powered by parallel inverters, a PWM method with a carrier phase shift of 90 degrees is proposed, which makes the phases of the harmonics at two times the carrier frequency in the two sets of three-phase windings opposite, effectively reducing HF vibration acceleration. Literature [9] sets a 180-degree phase shift on the carrier of the dual three-phase inverter, so that the harmonic phases at odd multiples of the carrier frequency in the two sets of three-phase windings are opposite, which reduces the HF vibration of the motor.

However, the above methods all rely on the cancellation of HF components in the magnetomotive force generated by the dual three-phase windings. This requires special designs such as common slots or interval slots for the dual three-phase windings of the motor, which severely limits the methods when extended to other types of motors.

In short, current researches usually focus on the frequency and magnitude of EM force, ignoring the influence of the spatial order of EM force on vibration. There lacks research on vibration reduction by adjusting the order of EM force.

This paper proposes a carrier phase shifted method for 4*3-phase PMSMs. The order of EM force is adjusted by carrier phase shift to suppress vibration. Firstly, the 4-module 3-phase PMSM and drive system were introduced, along with the analysis of the ① M force. Then the vibration reduction mechanism of CPS-PWM was explained theoretically, considering the orders of HF EM forces. Finally, experimental results are agreed with the prediction of the theory and indicate that this approach can significantly reduce HF vibration under certain conditions.

II. THE MODEL OF 4-MODULE 3-PHASE PMSM

Fig. 1 shows the structure of the 4- module 3-phase PMSM. The motor has four sets of windings which occupy four sectors of the stator respectively. So the mutual inductance among different sets of windings is small. The electrical angles of different sets of windings differ by 0° .

INTRODUCTION

Multiphase PMSMs fed by converters are widely used in energy conversion areas requiring high reliability like electric propulsion applications, due to the excellent fault tolerance capability[1-4]. However, when the converter is working under PWM, high-frequency harmonic currents are introduced into the stator windings, resulting in high-frequency(HF) electromagnetic(EM) force, and HF vibration, which destroys the stealth performance of the propulsion system.

In order to reduce the high frequency EM vibration introduced by the converter, many scholars have carried out research work from the perspective of changing the carrier frequency. Literature [5] pointed out that by changing the carrier frequency to avoid the natural frequency of the motor, HF vibration can be avoided. But for different motors, it is very difficult to select an appropriate carrier frequency. Literature [6] proposed a variable carrier frequency PWM strategy based on the rotor position, which broadened the harmonic current spectrum by changing the carrier frequency to reduce the value of HF harmonic current, and suppress the HF vibration. However, because these methods generally lack accurate analysis of motor vibration response, the variable carrier frequency may sometimes worsen the HF vibration [7].

Some scholars have also explored how to reduce HF vibration at a fixed carrier frequency. In reference [8], for dual

16

This work was supported in part by the National Science and Foundation of China under Grant 52077088. (*Corresponding author: Haiyang Fang*)

> REPLACE THIS LINE WITH YOUR MANUSCRIPT ID NUMBER (DOUBLE-CLICK HERE TO EDIT) <

2

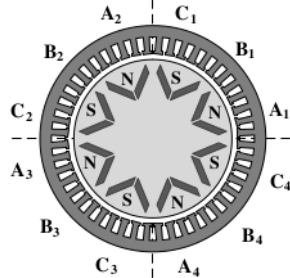
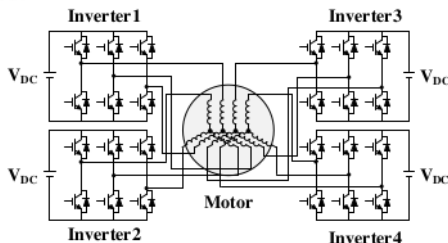
**Fig. 1.** Structure of the 4-module 3-phase PMSM

Fig. 2 shows the 4-module PMSM drive system. The system consists of four sets of three-phase voltage source inverters(VSIs) and a 4-module PMSM. Each set of windings of the motor is fed by a three-phase VSIs respectively. Therefore, each set of windings can be independently controlled.

**Fig. 2.** Schematic of 4-module PMSM drive system

III. ANALYSIS OF HIGH-FREQUENCY ELECTROMAGNETIC FORCE OF PMSM

The HF EM vibration of the motor is mainly generated by the HF EM force acting on the stator [10]. For PMSM, the HF EM force induced by PWM can be expressed as [11]:

$$f_{pwm}(\theta, t) = \sum_v \sum_{\omega} f_{v,\omega} \cos(v\theta - \omega t + \varphi) \quad (1)$$

$$v = 0, 2p \quad (2)$$

$$\omega = m\omega_c \pm n\omega_o (m \geq 1, n \geq 0) \quad (3)$$

$$\varphi = m\theta_c \pm n\theta_o \quad (4)$$

where v , ω and φ stand for the spatial order, angular frequency and phase of the EM force, respectively. p is the pole pairs number of the motor. ω_c and ω_o are the angular frequencies of the carrier and modulation wave, respectively. m , n are the index coefficient of the carrier and modulation wave. θ_c and θ_o are the phase of the carrier and modulation wave, respectively.

Formula (2) shows the spatial distribution of the force. It should be noted that: Formula (2) only applies to integer slot motors. For fractional slot motors, the spatial order of the HF EM force is very complex, which needs to be analyzed in combination with the specific motor structure.

Formula (3) shows the frequency characteristics of HF EM force under the Sinusoidal PWM(SPWM): concentrated on integral multiples of the carrier frequency. In Formula (3), when m is odd, n is $1, 3, 5, 7, 9, \dots$. When m is even, n is

$0, 2, 4, 6, 8, \dots$. That can be expressed as:

$$\left\{ \begin{array}{l} \omega = \omega_c \pm \omega_o, \omega_c \pm 3\omega_o, \dots \\ \omega = 2\omega_c, 2\omega_c \pm 2\omega_o, \dots \\ \dots \end{array} \right. \quad (5)$$

Formula (4) shows the phase characteristics of HF EM force. It can be seen from Formula (4) that the phase of the EM force can be changed by changing the phase of the carrier. The phase of the carrier changes X , the phase of EM force at m times the carrier frequency(mf_c) changes mX .

IV. THE MECHANISM OF VIBRATION GENERATION AND REDUCTION

A. Theoretical Analysis

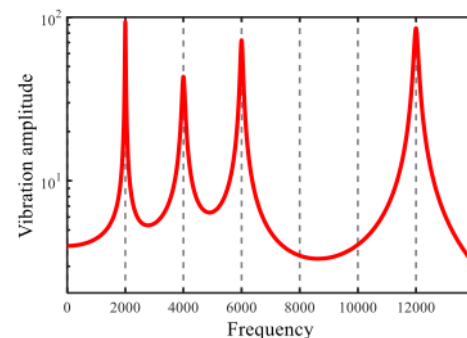
Fig. 3 shows a typical mechanical transfer function curve of the motors. It can be obtained by modal experiment or finite element simulation. Decomposing the mechanical transfer function, the mechanical transfer function curve of each order mode can be obtained, as shown in Fig. 4.

The v -order transfer function in Fig. 4 can be expressed as:

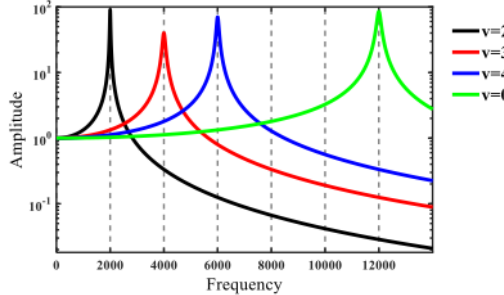
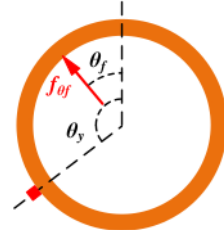
$$H(v, \omega) = \frac{I}{\left[\left(\frac{\omega}{\omega_v} \right)^2 - 1 \right] + 2\zeta_v \frac{\omega}{\omega_v} i} = |H(v, \omega)| e^{j\theta_{v,w}} \quad (6)$$

$$|H(v, \omega)| = \sqrt{\left(\frac{\omega}{\omega_v} \right)^2 - 1 + \left(2\zeta_v \frac{\omega}{\omega_v} \right)^2} \quad (7)$$

where ω_v and ζ_v are the natural frequency and damping ratio of the v -order mode, respectively. Obviously the overall mechanical transfer function in Fig. 3 can be expressed as $\sum_v H(v, \omega)$.

**Fig. 3.** Overall mechanical transfer function curve

> REPLACE THIS LINE WITH YOUR MANUSCRIPT ID NUMBER (DOUBLE-CLICK HERE TO EDIT) <

**Fig. 4.** Decomposed mechanical transfer function curve**Fig. 17.** Schematic diagram of the forces on the stator
In order to simplify the analysis, the motor stator is simplified as a ring, as shown in Fig. 5.

From Formula (1), it can be known that the μ -order HF EM force density can be expressed as:

$$f_\mu = f_{m\mu} \cos(\mu\theta - \omega t + \varphi_\mu) \quad (8)$$

As shown in Fig. 5, the EM force at point θ_f is expressed as :

$$f_{\theta_f} = f_{m\mu} \cos(\mu\theta_f - \omega t + \varphi_\mu) d\theta_f \quad (9)$$

The vibration response it produces at point θ_y is:

$$\begin{aligned} y &= f_{\theta_f} \times \sum_v H(v, \omega) \\ &= f_{m\mu} \cos(\mu\theta_f - \omega t + \varphi_\mu) d\theta_f \times \sum_v H(v, \omega) \\ &= \sum_v f_{m\mu} |H(v, \omega)| \cos[\mu\theta_f + v(\theta_y - \theta_f) - \omega t + \varphi_{u,v,\omega}] d\theta_f \end{aligned} \quad (10)$$

The vibration response produced by the total μ -order EM force at point θ_y is:

$$\begin{aligned} Y &= \int_0^{2\pi} \sum_v f_{m\mu} |H(v, \omega)| \cos[\mu\theta_f + v(\theta_y - \theta_f) - \omega t + \varphi_{u,v,\omega}] d\theta_f \\ &= \sum_v f_{m\mu} |H(v, \omega)| \int_0^{2\pi} \cos[\mu\theta_f + v(\theta_y - \theta_f) - \omega t + \varphi_{u,v,\omega}] d\theta_f \end{aligned} \quad (11)$$

when $\mu \neq v$:

$$\begin{aligned} f_{m\mu} |H(v, \omega)| \int_0^{2\pi} \cos[\mu\theta_f + v(\theta_y - \theta_f) - \omega t + \varphi_{u,v,\omega}] d\theta_f \\ = f_{m\mu} |H(v, \omega)| \int_0^{2\pi} \cos[(\mu - v)\theta_f + v\theta_y - \omega t + \varphi_{u,v,\omega}] d\theta_f \\ = f_{m\mu} |H(v, \omega)| \times 0 \\ = 0 \end{aligned} \quad (12)$$

That is, the v -order mode must be excited by the same order of EM force to generate vibration [12].

Therefore, Formula (11) can be simplified as:

$$\begin{aligned} Y &= f_{m\mu} |H(\mu, \omega)| \int_0^{2\pi} \cos[\mu\theta_f + \mu(\theta_y - \theta_f) - \omega t + \varphi_{u,v,\omega}] d\theta_f \\ &= 2\pi f_{m\mu} |H(\mu, \omega)| \cos(\mu\theta_y - \omega t + \varphi_{u,v,\omega}) \end{aligned} \quad (13)$$

The EM force with multiple spatial orders can be expressed as:

$$\begin{aligned} F &= \sum_\mu f_\mu \\ &= \sum_\mu f_{m\mu} \cos(\mu\theta - \omega t + \varphi_\mu) \end{aligned} \quad (14)$$

Combined with Formula (13), the vibration it generates at point θ_y can be expressed as:

$$\begin{aligned} Y &= \sum_\mu 2\pi f_{m\mu} |H(\mu, \omega)| \cos(\mu\theta_y - \omega t + \varphi_{u,v,\omega}) \\ &= \sum_\mu |Y_\mu| \cos(\mu\theta_y - \omega t + \varphi_{u,v,\omega}) \end{aligned} \quad (15)$$

$$|Y_\mu| = 2\pi f_{m\mu} |H(\mu, \omega)| \quad (16)$$

B. The Mechanism of Vibration Reduction:

For the HF EM force with frequency f_s , spatial order 0, and amplitude f_m , the vibration amplitude it produces is:

$$|Y_0| = 2\pi f_m |H(0, \omega_s)| \quad (17)$$

Change the order of the EM force, for example: change the order of the EM force to 2 without changing its amplitude and frequency, the vibration amplitude generated by it is:

$$|Y_2| = 2\pi f_m |H(2, \omega_s)| \quad (18)$$

When the EM force frequency f_s is close to the 0-order mode natural frequency f_{n0} , it can be seen from Fig. 4 that:

$$|H(0, \omega_s)| = |H(0, \omega_{n0})| \square |H(2, \omega_{n0})| = |H(2, \omega_s)| \quad (19)$$

$$2\pi f_m |H(0, \omega_s)| \square 2\pi f_m |H(2, \omega_s)| \quad (20)$$

$$|Y_0| \square |Y_2| \quad (21)$$

That is, by changing the order of the EM force, the vibration generated by it would be greatly reduced.

V. CARRIER PHASE SHIFTED PWM AND VIBRATION REDUCTION

A. How Carrier Phase Shifted PWM Changes the Order of the Electromagnetic Force:

It can be seen from Chapter 1 that each module of the 4-module 3-phase motor is independent of each other, so the EM force generated by each module is also decoupled. Therefore, by changing the phase of the carrier of each module, the phase of the EM force generated by each module is changed.

As shown in Fig. 6, taking the carrier of the first module as a reference, set the carrier phases of the second to fourth module as θ_2 , θ_3 , θ_4 , and record this carrier phase combination(CPC) as $0 - \theta_2 - \theta_3 - \theta_4$.

It can be seen from Formula (4) that when the CPC is $0 - \frac{180}{m}$, the phase combination of EM force at around mf_c is $0 - \frac{180}{m}$, the phase combination of EM force at around mf_c is $0 - \frac{180}{m}$

> REPLACE THIS LINE WITH YOUR MANUSCRIPT ID NUMBER (DOUBLE-CLICK HERE TO EDIT) <

4

180-0-180. At this time, the order of EM force at around mf_c changes from 0 to 2, as shown in Fig. 7.

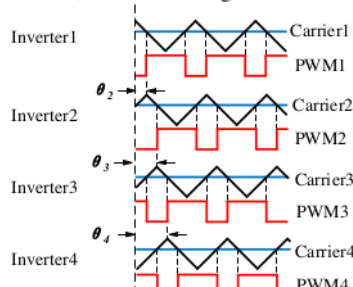


Fig. 6. Schematic diagram of CPS-PWM

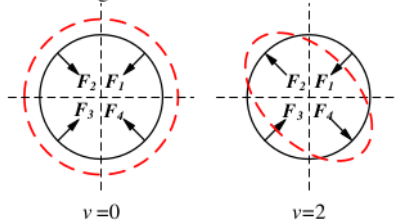


Fig. 7. Change of the order of the EM force

B. The Relationship between the Electromagnetic Force Order and the Carrier Phase Combination

It can be seen from Formula (2) that before the CPS-PWM is used, the main orders of the electromagnetic force are 0-order and $2p$ -order. The higher the order, the smaller the vibration generated by the EM force[13]. Therefore, the $2p$ -order electromagnetic force is ignored, and it is considered that the electromagnetic force is all 0-order before using the CPS-PWM. So the EM force can be expressed as:

$$\begin{aligned} f_{pwm} &= f_m \cos(\vartheta - \omega t + \varphi) \\ &= f_m \cos(0\theta - \omega t + m\theta_c \pm n\theta_b + \theta_o) \quad (22) \\ &= f_m \cos(-\omega t + m\theta_c + \theta_{o,n}) \end{aligned}$$

Next, the order 17 angle of the electromagnetic force is mainly analyzed. In order to simplify the analysis, the time variable t is ignored. Take $t=t_0$ so that:

$$f_{pwm} = f_m \cos(-\omega t_0 + m\theta_c + \theta_{o,n}) = f_m \quad (23)$$

For the EM force with frequency $m\omega_c \pm n\omega_b$, when the CPC is 0-X-0-X, its expression at time t_0 is:

$$\begin{cases} f_{pwm} = f_m & \theta \in [0, 90^\circ] \\ f_{pwm} = f_m \cos(mX) & \theta \in [90, 180^\circ] \\ f_{pwm} = f_m & \theta \in [180, 270^\circ] \\ f_{pwm} = f_m \cos(mX) & \theta \in [270, 360^\circ] \end{cases} \quad (24)$$

The amplitude of each order EM force can be obtained by performing fast Fourier transform(FFT) on Formula (24). And Formula (24) can also be expressed as:

$$\begin{aligned} f_{pwm} &= f_{m0} + f_{m1} \cos(\theta) + f_{m2} \cos(2\theta) + \dots \\ &= \sum_{\mu} f_{m\mu} \cos(\mu\theta) \quad (25) \end{aligned}$$

Although there are many kinds of CPCs, after analysis, only two kinds of CPCs are helpful for vibration suppression: 0-X-0-X and 0-0-X-X.

Fig. 8 and Fig. 9 show that when CPC is 0-X-0-X and 0-0-X-X, the relative amplitude of each order EM force at around mf_c varies with the carrier phase angle(CPA).

As shown in Fig. 8, when the CPS is 0-X-0-X, the order of the EM force is expressed as: $\mu = 0, 2, 6, 10, \dots$. The relative amplitude of the 0-order EM force decreases sinusoidally with the CPA X, and the relative amplitudes of the other-order EM forces increase sinusoidally with the CPA X. When the CPA X is 180° , the amplitude of the 0-order EM force is 0 and the 2-order EM force is dominant.

As shown in Fig. 9, when the CPS is 0-0-X-X, the order of the EM force is expressed as: $\mu = 0, 1, 3, 5, \dots$. In general, there is no 1-order mode of the motor[14], so the vibration generated by the 1-order EM force can be ignored. Therefore, ignoring the 1-order EM force, it is considered that when the CPA is 180° , the 3-order EM force is dominant.

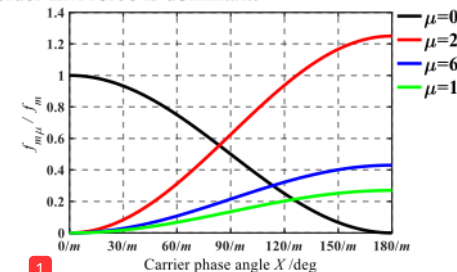


Fig. 8. Change of orders under CPC 0-X-0-X

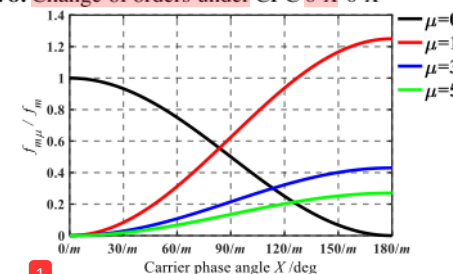


Fig. 9. Change of orders under CPC 0-0-X-X

VI. EXPERIMENTAL VALIDATION

To verify the above analysis, experiments are conducted on three different PMSMs, which are a 4-module PMSM(motor 1) with 48 slots and 8 poles, a 2-module PMSM(motor 2) with 12 slots and 8 poles, and a 4-module PMSM(motor 3) with 12 slots and 16 poles. The following three groups of experiments are described in details:

A. Introduction to the experimental platform:

The structures of the three motors are shown in Fig. 10, Fig. 11 and Fig. 12. The basic parameters are shown in Table I, Table II and Table III.

> REPLACE THIS LINE WITH YOUR MANUSCRIPT ID NUMBER (DOUBLE-CLICK HERE TO EDIT) <

The experimental platform are shown in Fig. 13. Accelerometers are evenly arranged on the stator surface. Control the motor to run at a constant speed, measure the vibration acceleration, and obtain the vibration spectrums after analysis. Take the average of the vibration amplitudes measured by all sensors as the vibration result. Change the carrier frequency and CPCs, repeat the above steps, then compare the vibration results under different conditions.

The harmonic current at around $2f_c$ generated by the VSIs is the largest[15], so the vibration at around $2f_c$ is generally the largest. Therefore, focus on the change of the vibration at around $2f_c$.

Set the CPA X to 0° , 10° , 10° ..., 90° , so that the phase of the EM force at around $2f_c$ changes from 0° to 180° .

The carrier frequency is taken as half of the natural frequency of the 0-order mode and the 3-order mode, which makes the vibration change obvious.

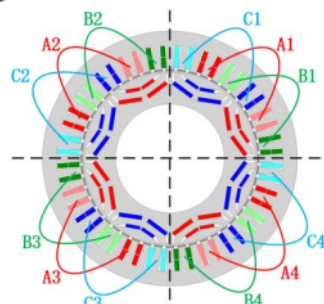


Fig. 10. Structure diagram of motor 1

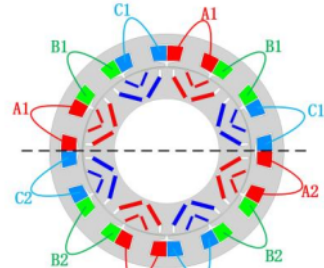


Fig. 11. Structure diagram of motor 2

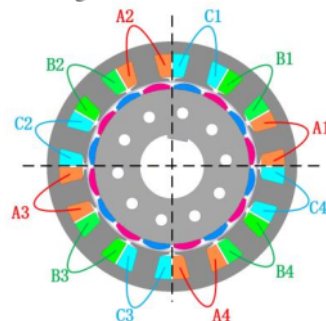


Fig. 12. Structure diagram of motor 3
TABLE I

PARAMETERS OF MOTORS

Parameter	Motor1	Motor2	Motor3
Slot number	48	12	12
Pole number	8	8	16
Stator OD(mm)	180	180	124
Stator ID(mm)	124	130	85
Air gap(mm)	0.8	0.8	1.4
Rated power(kW)	15.67	15.77	3
Rated speed(rpm)	3000	3000	1000

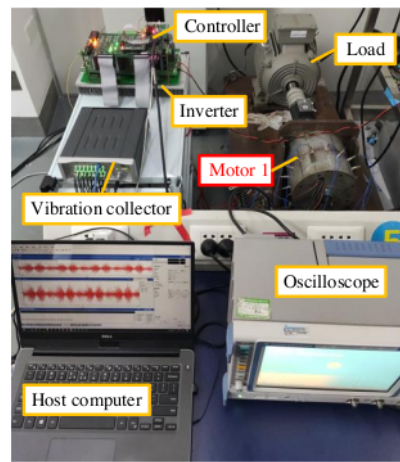


Fig. 13. Experimental platform for motors

B. Experimental results of motor 1:

The modal experiment is carried out on the motor, and the natural frequencies of the motor are shown in Table II.

TABLE II

NATURAL FREQUENCY OF MOTOR 1

Order	Natural Frequency/Hz
2	1990
3	3042
4	4577
0	20127

Fig. 14 shows the vibration spectrums under CPC 0-0-0 and CPC 0-90-0-90 when the carrier frequency is 10kHz. It can be seen from the spectrums that the vibration amplitude at around $2f_c$ is the largest. Comparing the two spectrums, we can see that in the case of 0-90-0-90, the vibration amplitude at around $2f_c$ is reduced by about 50%.

When $f_c = 10\text{kHz}$, there exists $2f_c \approx f_{n0}$, where f_{n0} is the 0-order mode natural frequency.

$$\text{Therefore : } |H(0,2\omega_c)| \gg |H(3,2\omega_c)| > |H(2,2\omega_c)| .$$

When CPC is 0-0-0-0, the theoretical vibration amplitude around $2f_c$ is $|Y_{0-0-0-0}| = f_{m0} |H(0,2\omega_c)| = f_m |H(0,2\omega_c)|$.

When CPC is 0-90-0-90, the theoretical vibration amplitude around $2f_c$ is

> REPLACE THIS LINE WITH YOUR MANUSCRIPT ID NUMBER (DOUBLE-CLICK HERE TO EDIT) <

6

$$\begin{aligned}|Y_{0-90-0-90}| &= |f_{m2}H(2,2\omega_c)| + |f_{m6}H(6,2\omega_c)| + |f_{m10}H(10,2\omega_c)| + \dots \\ &\approx f_{m2}|H(2,2\omega_c)| \\ &= 1.25f_m|H(2,2\omega_c)|\end{aligned}$$

Since $|H(0,2\omega_c)| \gg |H(2,2\omega_c)|$, so $|Y_{0-0-0-0}| \gg |Y_{0-90-0-90}|$.

Therefore, the vibration amplitude at around $2f_c$ is reduced in the case of 0-90-0-90.

It can be seen from Fig. 14 that the vibration is reduced by about 50%, and the vibration reduction effect is not as good as the theoretical analysis. This is mainly because: In the theoretical analysis, the motor stator is regarded as an ring without thickness. But the actual motor has a casing, coils, and it is a slotted design, which make the motor stator unable to be regarded as an ideal ring and affect the vibration reduction effect.

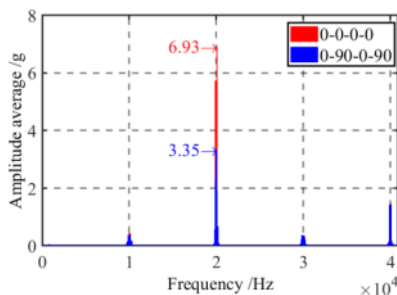


Fig. 14. Vibration spectrum when $f_c = 10\text{kHz} \approx f_{n0}/2$

Fig. 15 shows the vibration amplitudes at around $2f_c$ under different CPCs when the carrier frequency is 10kHz. As can be seen from the figure, as the CPA X increases, the vibration amplitude gradually decreases. In the case of the same CPA X, the vibration amplitude under 0-X-0-X is smaller than that under 0-0-X-X.

The vibration at around $2f_c$ can be expressed as:

$$\begin{aligned}|Y_{0-X-0-X}| &= f_{m0}|H(0,2\omega_c)| + f_{m2}|H(2,2\omega_c)| + f_{m6}|H(6,2\omega_c)| \dots \quad (26) \\ &\approx f_{m0}|H(0,2\omega_c)| + f_{m2}|H(2,2\omega_c)|\end{aligned}$$

$$\begin{aligned}|Y_{0-0-X-X}| &= f_{m0}|H(0,2\omega_c)| + f_{m1}|H(1,2\omega_c)| + f_{m3}|H(3,2\omega_c)| \dots \quad (27) \\ &\approx f_{m0}|H(0,2\omega_c)| + f_{m3}|H(3,2\omega_c)|\end{aligned}$$

As shown in Fig. 8 and Fig. 9, as the CPA X increases, the magnitude of the 0-order EM force f_{m0} gradually decreases, so the first term in Formula (26),(27) gradually decreases. Therefore, the vibration at $2f_c$ also decreases gradually.

Since $|H(2,2\omega_c)| < |H(3,2\omega_c)|$, the second term in Formula (26) is less than that in Formula (27), so the vibration amplitude under 0-X-0-X is smaller than that under 0-0-X-X.

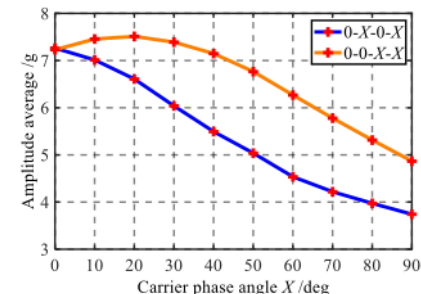


Fig. 15. Vibration Amplitude at around $2f_c$ versus CPA when $f_c = 10\text{kHz} \approx f_{n0}/2$

Fig. 16 shows the vibration spectrums under CPC 0-0-0-0 and CPC 0-0-90-90 when the carrier frequency is 1500Hz. We can see that in the case of 0-0-90-90, the vibration amplitude at around $2f_c$ increased by 30 times.

When $f_c = 1500\text{Hz}$, there are: $2f_c \approx f_{n3}$, where f_{n0} is the 0-order mode natural frequency.

$$\text{Therefore : } |H(3,2\omega_c)| \gg |H(2,2\omega_c)| \gg |H(0,2\omega_c)| .$$

When CPC is 0-0-0-0, the theoretical vibration amplitude at around $2f_c$ is $|Y_{0-0-0-0}| = f_{m0}|H(0,2\omega_c)| = f_m|H(0,2\omega_c)|$.

When CPC is 0-0-90-90, the theoretical vibration amplitude at around $2f_c$ is

$$\begin{aligned}|Y_{0-90-90}| &= |f_{m1}H(1,2\omega_c)| + |f_{m3}H(3,2\omega_c)| + |f_{m5}H(5,2\omega_c)| + \dots \\ &\approx f_{m3}|H(3,2\omega_c)| \\ &= 0.43f_m|H(3,2\omega_c)|\end{aligned}$$

Since $|H(3,2\omega_c)| \gg |H(0,2\omega_c)|$, so $|Y_{0-90-90}| \gg |Y_{0-0-0-0}|$.

Therefore, the vibration amplitude at around $2f_c$ is greatly increased in the case of 0-0-90-90.

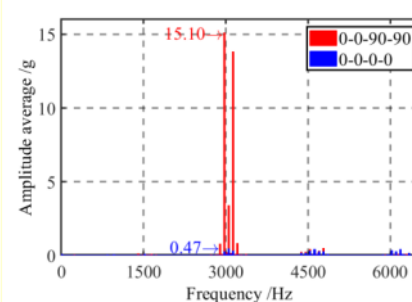


Fig. 16. Vibration spectrum when $f_c = 1500\text{Hz} \approx f_{n3}/2$

Fig. 17 shows the vibration amplitudes at around $2f_c$ under different CPCs when the carrier frequency is 1500Hz. As can be seen from the figure, as the CPA X increases, the vibration amplitude gradually increases. In the case of the same CPA X, the vibration amplitude under 0-X-0-X is smaller than that under 0-0-X-X.

Since $|H(3,2\omega_c)| \gg |H(2,2\omega_c)| \gg |H(0,2\omega_c)|$, the vibration at around $2f_c$ can be expressed as :

> REPLACE THIS LINE WITH YOUR MANUSCRIPT ID NUMBER (DOUBLE-CLICK HERE TO EDIT) <

$$|Y_{0-X,0,X}| = f_{m0} |H(0,2\omega_c)| + f_{m2} |H(2,2\omega_c)| + f_{m6} |H(6,2\omega_c)| \dots \quad (28)$$

$$\approx f_{m2} |H(2,2\omega_c)|$$

$$|Y_{0-X,X,X}| = f_{m0} |H(0,2\omega_c)| + f_{m1} |H(1,2\omega_c)| + f_{m3} |H(3,2\omega_c)| \dots \quad (29)$$

$$\approx f_{m3} |H(3,2\omega_c)|$$

16

As shown in Fig. 8 and Fig. 9, as the CPA X increases, f_{m2} and f_{m3} gradually increase. Therefore, the vibration at $2f_c$ also decreases gradually.

Since $|H(2,2\omega_c)| < |H(3,2\omega_c)|$, so the vibration amplitude under 0-X-0-X is smaller than that under 0-0-X-X.

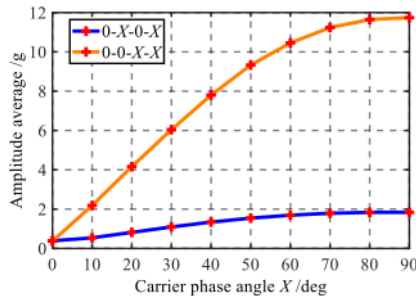


Fig. 17. Vibration Amplitude at around $2f_c$ versus CPA when $f_c = 1500\text{Hz} \approx f_{n3}/2$

C. Experimental results of 12-slot 8-pole motor:

The modal experiment is carried out on the motor, and the natural frequencies of the motor are shown in Table III.

TABLE III

NATURAL FREQUENCY OF MOTOR 2

Order	Natural Frequency/Hz
2	2394
3	3434
4	5428
0	25207

The motor is a 2-module motor, so there is only one type of CPC, namely 0-X. It can be seen from the motor structure in Fig. 11 that 0-X in the two-module motor can be equivalent to 0-0-X-X in the four-module motor.

Experiments were carried out when the carrier frequency was 1700 Hz and 12500 Hz. The experimental results are shown in Fig. 18, Fig. 19 and are very similar to the experimental results of motor A.

The motor used is a fractional slot concentrated winding motor, and the spatial order of the EM force is relatively complex, not only containing 0-order. However, it can be seen from Fig. 18 that the vibration can still be reduced by using CPS-PWM, although the vibration suppression effect is not as good as that of integer slot motors. 1

Similarly, when the carrier frequency of 2 times is close to the natural frequency of the 3-order mode, using the CPS-PWM, the HF vibration is greatly increased.

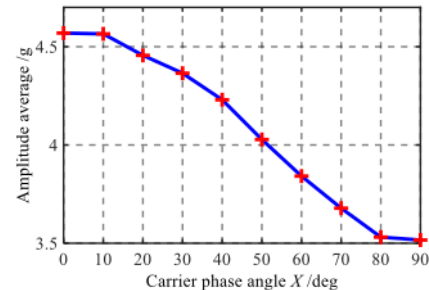


Fig. 18. Vibration Amplitude at around $2f_c$ versus CPA when $f_c = 12.5\text{kHz} \approx f_{n0}/2$

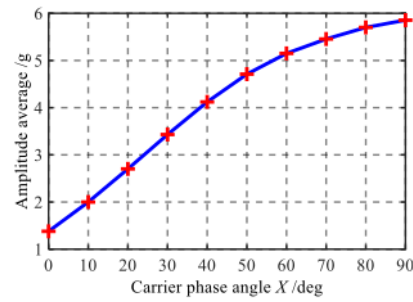


Fig. 19. Vibration Amplitude at around $2f_c$ versus CPA when $f_c = 1700\text{Hz} \approx f_{n3}/2$

D. Experimental results of 12-slot 16-pole motor:

The modal experiment is carried out on the motor, and the natural frequencies of the motor are shown in Table IV.

TABLE IV

NATURAL FREQUENCY OF MOTOR 3

Order	Natural Frequency/Hz
2	2312
3	3263
4	4940
0	18137

Experiments were carried out when the carrier frequency was 1600 Hz and 9000 Hz. The experimental results are shown in Fig. 20, Fig. 21 and are very similar to the experimental results of motor 1.

The motor used is a fractional slot concentrated winding motor, and each module contains two pairs of magnetic poles. However, it can be seen from Fig. 20 that the vibration can still be reduced by using CPS-PWM.

Through the above three sets of motor experiments, it can be seen that the structure of the PMSM does not affect the vibration suppression effect of CPS-PWM. As long as the motor is a multi-module PMSM, the HF EM vibration can be suppressed by using the proper CPS-PWM.

> REPLACE THIS LINE WITH YOUR MANUSCRIPT ID NUMBER (DOUBLE-CLICK HERE TO EDIT) <

8

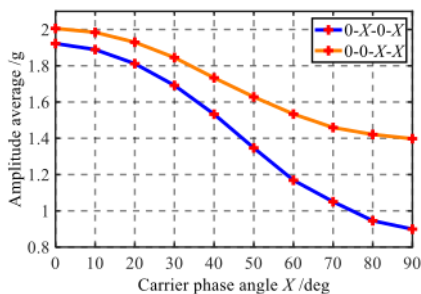


Fig. 20. Vibration Amplitude at around $2f_c$ versus CPA when $f_c = 9000\text{Hz} \approx f_{n0} / 2$

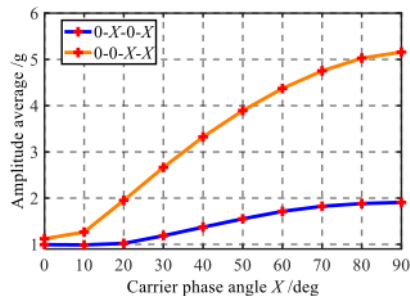


Fig. 21. Vibration Amplitude at around $2f_c$ versus CPA when $f_c = 1600\text{Hz} \approx f_{n3} / 2$

VII. CONCLUSION

This paper provides a new HF PWM EM vibration suppression method, which can suppress vibration by changing the order of the EM force. In this paper, the principle of vibration suppression is theoretically analyzed, and the effectiveness of the method is verified by experiments. The following conclusions can be drawn.

- 1) At a specific carrier frequency, that is, when the carrier frequency multiplier is close to the 0-order mode natural frequency, the HF vibration of the multi-module motor can be effectively reduced by using proper CPS-PWM. However, when the carrier frequency multiplier is close to the natural frequency of the 2-order or 3-order mode, the HF vibration may increase under CPS-PWM.
- 2) The 0-order EM force can be transformed to the 2-order or 3-order force by the CPS-PWM of 0-X-0-X or 0-0-X-X. The order of the main EM force under 0-X-0-X is lower, so 0-X-0-X is better at HF vibration reduction.
- 3) This vibration suppression method is suitable for multi-module PMSMs and is not affected by the structure of the stator or rotor. But the EM force order distribution of integer slot motor is relatively simple, and therefore the vibration suppression effect of integer slot motor is better.

ACKNOWLEDGMENT

This work is supported by the National Natural Science Foundation of China under Project 52077088.

REFERENCES

- [1] S. Yan, Q. Wang, Y. Xu, Z. Liu, H. Fang and D. Jiang, "Research on High Frequency Vibration Reduction Using Carrier Phase Shifted PWM for 4 3-Phase Windings Permanent Magnet Synchronous Motor," in 2021 IEEE Energy Conversion Congress and Exposition (ECCE), Vancouver, BC, Canada, 2021, pp. 4468-4472.
- [2] A. Mohammadiour and L. Parsa, "Global Fault-Tolerant Control Technique for Multiphase Permanent-Magnet Machines," in IEEE Transactions on Industry Applications, vol. 51, no. 1, pp. 178-186, Jan.-Feb. 2015.
- [3] Z. Liu, L. Fang, D. Jiang and R. Qu, "A Machine-learning Based Fault Diagnosis Method with Adaptive Secondary Sampling for Multiphase Five Systems," in IEEE Transactions on Power Electronics.
- [4] X. Peng, Z. Liu, and D. Jiang, "A review of multiphase energy conversion in wind power generation," Renewable and Sustainable Energy Reviews, vol. 11, 147, p. 111172, Sep. 2021.
- [5] E. Zeze, and K. Akatsu, "Research on vibration analysis and noise-reduction technique of PM motor," in 2012 XXth International Conference on Electrical Machines, Marseille, 2012, pp. 458-463.
- [6] Zhi Yang, S. Yaman and M. Krishnamurthy, "Mitigation of EM vibration in PMSM: A rotor position related variable carrier frequency technique," in 2017 IEEE Transportation Electrification Conference and Expo (ITEC), Chicago, IL, 2017, pp.448-452.
- [7] I. P. Tsoumas, and H. Tischmacher, "Influence of the inverter's modulation technique on the audible noise of electric motors," in 2012XXth International Conference on Electrical Machines, Marseille 2012, pp. 2981-2987.
- [8] F. Yuan, S. Huang, and Q. Hao, "Research on High Frequency Vibration Suppression of Permanent Magnet Motor Using Carrier Phase Shift Technology," in Electric Machines and Control, 2014, (7):12-17.
- [9] W. Zhang, Y. Xu, H. Huang and J. Zou, "Vibration Reduction for Dual-Branch Three-Phase Permanent Magnet Synchronous Motor With Carrier Phase-Shift Technique," in IEEE Transactions on Power Electronics, vol. 35, no. 1, pp. 607-618, Jan. 2020.
- [10] X. Li, C. Liu, and B. Mei, "Analysis of Vibration and Noise Source of Electric Vehicle IPMSM Wide Range Speed Regulation," in Electric Machines and Control, 2018, 38(17):5219-5227+5319.
- [11] C. Liao, W. Jiang and Z. Zhang, "Analysis of EMVibration Characteristics of An Interior Permanent Magnet Synchronous Motor," in 2019 22nd International Conference on Electrical Machines and Systems (ICEMS), Haikou, China, 2019, pp.1-5.
- [12] S. Wang, J. Hong, Y. Sun and H. Cao, "Analysis of Zeroth-Mode Slot Frequency Vibration of Integer Slot Permanent-Magnet Synchronous Motors," in IEEE Transactions on Industrial Electronics, vol. 67, no. 4, pp. 2654-2664, April 2020.
- [13] Y. -S. Lai, W. -T. Lee, Y. -K. Lin and J. -F. Tsai, "Integrated Inverter/Converter Circuit and Control Technique of Motor Drives With Dual-Mode Control for EV/HEV Applications," in IEEE Transactions on Power Electronics, vol. 29, no. 3, pp. 1358-1365, March 2014.
- [14] G. Vidmar and D. Miljavec, "A Universal High-Frequency Three-Phase Electric-Motor Model Suitable for the Delta- and Star-Winding Connections," in IEEE Transactions on Power Electronics, vol. 30, no. 8, pp. 4365-4376, Aug. 2015.
- [15] Pulse Width Modulation for Power Converters Principles and Practice[M]. John Wiley & Sons Inc, 2003.



4

Zicheng Liu (M'18) was born in Shandong, China, in 1989. He received the B.S. degree in Hydropower Engineering from Huazhong University of Science and Technology (HUST), Wuhan, China, in 2011, and the Ph.D. degree in Electrical Engineering from Tsinghua University, Beijing, China, in 2016. During Oct. 2014 to Mar. 2015, he was a Visiting Student at Purdue University, West Lafayette, IN, USA. During Jun. 2016 to Sep. 2018, he was a postdoc researcher at Beijing Jiaotong University, Beijing, China. He is currently an associate professor at HUST. His research interests include multiphase motor control systems and transportation electrification.

> REPLACE THIS LINE WITH YOUR MANUSCRIPT ID NUMBER (DOUBLE-CLICK HERE TO EDIT) <



She Yan was born in Jiangxi, China, in 1999. He received the B.S. degree in Electrical Engineering from the Huazhong University of Science and Technology, Wuhan, China, in 2021, where he is currently working toward the M.S. degree in Electrical Engineering with the School of Electronic and Electrical Engineering. His main research interests are motor control and motor vibration.



Haiyang Fang (Member, IEEE) was born in Hubei, China. He received the B.M.E. degree in mechanical engineering and the Ph.D. degree in electrical engineering from the Huazhong University of Science and Technology, Wuhan, China, in 2013 and 2018, respectively. His research interests include mechanical design and vibro-acoustic analysis of electrical machines.



Dong Jiang (S05'-M12'-SM16') received B.S and M.S degrees in electrical engineering from Tsinghua University, Beijing, China, in 2005 and 2007 respectively. He began his Ph.D. study in Center for Power Electronics Systems (CPES) in Virginia Tech in 2007 and was transferred to University of Tennessee with his advisor in 2010. He received his Ph.D. degree in power electronics and motor drives from University of Tennessee in Dec. 2011. He was with United Technologies Research Center (UTRC) in Connecticut as a Senior Research Scientist/Engineer from Jan 2012 to July 2015. He has been with Huazhong University of Science &Technology (HUST) in China as a professor since July 2015. Dong Jiang's major research area is power electronics and motor drives, with more than 40 published IEEE journal and conference papers in this area. He has two best paper awards in IEEE conferences. He is an associate editor of IEEE Transactions on Industry Applications.



Ronghai Qu (Fellow, IEEE) was born in China. He received the B.E.E. and M.S.E.E. degrees in electrical engineering from Tsinghua University, Beijing, China, in 1993 and 1996, respectively, and the Ph.D. degree in electrical engineering from the University of Wisconsin-Madison, Madison, WI, USA, in 2002. In 1998, he joined the Wisconsin Electric Machines and Power Electronics Consortiums as Research Assistant. He became a Senior Electrical Engineer with Northland, a Scott Fetzer Company in 2002. Since 2003, he had been with the General Electric (GE) Global Research Center, Niskayuna, NY, USA, as a Senior Electrical Engineer with the Electrical Machines and Drives Laboratory. He has authored more than 120 published technical papers and is the holder of more than 50 patents/patent applications. From 2010, he has been a Professor with the Huazhong University of Science &Technology, Wuhan, China. Prof. Qu is a full member of Sigma Xi. He has been the recipient of several awards from GE Global Research Center since 2003, including the Technical Achievement and Management Awards. He is also the recipient of the 2003 and 2005 Best Paper Awards, and third prize from the Electric Machines Committee of the IEEE Industry Applications Society at the 2002 and 2004 IAS Annual Meeting.

Research on High Frequency Vibration Reduction Using Carrier Phase Shifted PWM for 4-module 3-Phase Permanent Magnet Synchronous Motor

ORIGINALITY REPORT

39%
SIMILARITY INDEX

19%
INTERNET SOURCES

39%
PUBLICATIONS

9%
STUDENT PAPERS

PRIMARY SOURCES

- 1 She Yan, Qiyuan Wang, Yunsong Xu, Zicheng Liu, Haiyang Fang, Dong Jiang. "Research on High Frequency Vibration Reduction Using Carrier Phase Shifted PWM for 4*3-Phase Windings Permanent Magnet Synchronous Motor", 2021 IEEE Energy Conversion Congress and Exposition (ECCE), 2021 Publication **17%**
- 2 Jingyi Liu, Xinggang Fan, Dawei Li, Ronghai Qu, Haiyang Fang. "Minimization of AC Copper Loss in Permanent Magnet Machines by Transposed Coil Connection", IEEE Transactions on Industry Applications, 2021 Publication **5%**
- 3 Dong Jiang, Kang Liu, Zicheng Liu, Qiyuan Wang, Zhongxiang He, Ronghai Qu. "Four-module Three-phase PMSM Drive for Suppressing Vibration and Common-mode Current", IEEE Transactions on Industry Applications, 2021 **3%**

4

Zicheng Liu, Xiangwen Sun, Zedong Zheng, Dong Jiang, Yongdong Li. "Optimized Current Trajectory Tracking Control of a Five-Phase Induction Machine Under Asymmetrical Current Limits", IEEE Transactions on Power Electronics, 2020

2%

Publication

5

Submitted to Virginia Polytechnic Institute and State University

2%

Student Paper

6

R. Sudharshan Kaarthik, P. Pillay. "Real-time power hardware-in-the-loop emulation of a parallel hybrid electric vehicle drive train", 2017 IEEE Transportation Electrification Conference (ITEC-India), 2017

1%

Publication

7

Zicheng Liu, Lanlan Fang, Dong Jiang, Ronghai Qu. "A Machine-learning Based Fault Diagnosis Method with Adaptive Secondary Sampling for Multiphase Drive Systems", IEEE Transactions on Power Electronics, 2022

1%

Publication

8

Wenzhe Deng, Shuguang Zuo. "Comparative Study of Sideband Electromagnetic Force in Internal and External Rotor PMSMs with SVPWM Technique", IEEE Transactions on Industrial Electronics, 2018

1%

Publication

-
- 9 nottingham-repository.worktribe.com 1 %
Internet Source
-
- 10 Jianfeng Hong, Shanming Wang, Yuguang Sun, Haixiang Cao. "A High-precision Analytical Method for Vibration Calculation of Slotted Motor Based on Tooth Modeling", IEEE Transactions on Industry Applications, 2021 1 %
Publication
-
- 11 Xiaohua Li, Yue Lu, Rongjian Zhao, Anhui Feng, Yudong Liu, Wenda He. "Electromagnetic Vibration and Noise Analysis of IPMSM for Electric Vehicles under Different Working Conditions", 2021 3rd International Conference on Smart Power & Internet Energy Systems (SPIES), 2021 1 %
Publication
-
- 12 Zaixin Song, Chunhua Liu, Hang Zhao. "Exact Multi-Physics Modelling and Experimental Validation of Spoke-Type Permanent Magnet Brushless Machines", IEEE Transactions on Power Electronics, 2021 1 %
Publication
-
- 13 Submitted to UT, Dallas 1 %
Student Paper
-
- 14 Cui Mingkai, Yu Yanjun. "Variable Parameter PI Control based on Fuzzy Logic Strategy for 1 %

Dual-Winding PMSM", 2021 IEEE 4th Student Conference on Electric Machines and Systems (SCEMS), 2021

Publication

-
- 15 Xun Han, Dong Jiang, Tianjie Zou, Ronghai Qu, Kai Yang. "Two-segment three-phase PMSM drive with carrier phase-shift PWM", 2018 IEEE Applied Power Electronics Conference and Exposition (APEC), 2018 <1 %
- Publication
-
- 16 pearl.shanghaitech.edu.cn <1 %
- Internet Source
-
- 17 tel.archives-ouvertes.fr <1 %
- Internet Source
-
- 18 www.ieee-ecce.org <1 %
- Internet Source
-
- 19 Haiyang Fang, Dawei Li, Jiaxiong Guo, Yunsong Xu, Ronghai Qu. "Hybrid Model for Electromagnetic Vibration Synthesis of Electrical Machines Considering Tooth Modulation and Tangential Effects", IEEE Transactions on Industrial Electronics, 2021 <1 %
- Publication
-
- 20 www.pcsee.org <1 %
- Internet Source
-
- 21 Minyu Cai, Tom Craddock, Oleg Wasynczuk. "High-frequency modeling, parameterization, 720/\$31.00 © 2021 IEEE <1 %

and simulation of IPM motor drive systems",
2017 IEEE Power and Energy Conference at
Illinois (PECI), 2017

Publication

-
- 22 Pengye Wang, Shang Gong, Xiangwen Sun, Zicheng Liu, Dong Jiang, Ronghai Qu. "Fault-tolerant reconfiguration topology and control strategy for symmetric open-winding multiphase machines", IEEE Transactions on Industrial Electronics, 2021 <1 %
- Publication
-
- 23 Dong Jiang, Kang Liu, Zicheng Liu, Qiyuan Wang, Zhongxiang He, Ronghai Qu. "Four-Module Three-Phase PMSM Drive for Suppressing Vibration and Common-Mode Current", IEEE Transactions on Industry Applications, 2021 <1 %
- Publication
-
- 24 Haiyang Fang, Dawei Li, Jiaxiong Guo, Yunsong Xu, Ronghai Qu. "Hybrid Model for Electromagnetic Vibration Synthesis of Electrical Machines Considering Tooth Modulation and Tangential Effects", IEEE Transactions on Industrial Electronics, 2020 <1 %
- Publication
-
- 25 Dongdong Chen, Wubin Kong, Ronghai Qu, Libing Zhou. "Correction of Field Orientation Inaccuracy Caused by Resolver Periodic Error" <1 %

and Rotor Time Constant Variation for Indirect Field-Oriented Control Induction Motor Drives", IEEE Transactions on Industrial Electronics, 2022

Publication

- 26 Guodong Feng, Chunyan Lai, Wenlong Li, Ze Li, Narayan C. Kar. "Dual Reference Frame based Current Harmonic Minimization for Dual Three-phase PMSM Considering Inverter Voltage Limit", IEEE Transactions on Power Electronics, 2020 <1 %
- Publication
-
- 27 Wentao Zhang, Yongxiang Xu, Yingliang Huang, Jibin Zou. "Reduction of high-frequency vibration noise for dual-branch three-phase permanent magnet synchronous motors", Chinese Journal of Electrical Engineering, 2020 <1 %
- Publication
-
- 28 Bifa Chen, Meian Zhang, Guo-an Tang. "Principle and experimental research on vibration reduction of flexible solar array using reaction flywheel", Aircraft Engineering and Aerospace Technology, 2018 <1 %
- Publication
-
- 29 Kristen Railey Kita, Supun Randeni, Dino DiBiaso, Henrik Schmidt. "Passive acoustic tracking of an unmanned underwater vehicle" <1 %

using bearing-Doppler-speed measurements",
The Journal of the Acoustical Society of
America, 2022

Publication

-
- 30 Wenzhe Deng, Shuguang Zuo. "Comparative Study of Sideband Electromagnetic Force in Internal and External Rotor PMSMs With SVPWM Technique", IEEE Transactions on Industrial Electronics, 2019 <1 %
- Publication
-
- 31 tii.ieee-ies.org <1 %
- Internet Source
-
- 32 Amir Farhang Sotoodeh, Farzin Ahmadi, Zahra Ghaffarpour, Mohammad Ebadollahi, Hossein Nasrollahi, Majid Amidpour. "Performance analyses of a waste-to-energy multigeneration system incorporated with thermoelectric generators", Sustainable Energy Technologies and Assessments, 2022 <1 %
- Publication
-
- 33 Niki Regina, Matteo Zanzi. "Camera Pan-Tilt Gimbals Robust Control Law for Target Tracking with Fixed Wing UAV", AIAA Guidance, Navigation, and Control (GNC) Conference, 2013 <1 %
- Publication
-
- 34 Wei Wang, Jinghao Zhang, Ming Cheng, Shihua Li. "Fault-Tolerant Control of Dual <1 %

Three-Phase Permanent-Magnet Synchronous Machine Drives under Open Phase Faults", IEEE Transactions on Power Electronics, 2016

Publication

Exclude quotes Off

Exclude bibliography Off

Exclude matches Off